

Learning quantum properties from short-range correlations using multi-task networks

Ya-Dong Wu,^{1,2} Yan Zhu,^{2,*} Yuexuan Wang,^{3,4} and Giulio Chiribella^{2,5,6,†}

¹*John Hopcroft Center for Computer Science, Shanghai Jiao Tong University, Shanghai 200240, China*

²*QICI Quantum Information and Computation Initiative, Department of Computer Science,
The University of Hong Kong, Pokfulam Road, Hong Kong*

³*AI Technology Lab, Department of Computer Science,
The University of Hong Kong, Pokfulam Road, Hong Kong*

⁴*College of Computer Science and Technology, Zhejiang University, Zhejiang Province, China*

⁵*Department of Computer Science, Parks Road, Oxford, OX1 3QD, United Kingdom*

⁶*Perimeter Institute for Theoretical Physics, Waterloo, Ontario N2L 2Y5, Canada*

Characterizing multipartite quantum systems is crucial for quantum computing and many-body physics. The problem, however, becomes challenging when the system size is large and the properties of interest involve correlations among a large number of particles. Here we introduce a neural network model that can predict various quantum properties of many-body quantum states with constant correlation length, using only measurement data from a small number of neighboring sites. The model is based on the technique of multi-task learning, which we show to offer several advantages over traditional single-task approaches. Through numerical experiments, we show that multi-task learning can be applied to sufficiently regular states to predict global properties, like string order parameters, from the observation of short-range correlations, and to distinguish between quantum phases that cannot be distinguished by single-task networks. Remarkably, our model appears to be able to transfer information learnt from lower dimensional quantum systems to higher dimensional ones, and to make accurate predictions for Hamiltonians that were not seen in the training.

I. INTRODUCTION

The experimental characterization of many-body quantum states is an essential task in quantum information and computation. Neural networks provide a powerful approach to quantum state characterization [1–4], enabling a compact representation of sufficiently structured quantum states [5]. In recent years, different types of neural networks have been successfully utilized to predict properties of quantum systems, including quantum fidelity [6–8] and other measures of similarity [9, 10], quantum entanglement [11–13], entanglement entropy [1, 14, 15], two-point correlations [1, 2, 14, 16] and Pauli expectation values [4, 17], as well as to identify phases of matter [18–22].

A challenge in characterizing multiparticle quantum systems is that important properties, such as topological invariants characterizing different quantum phases of matter [23], are global: their direct estimation requires measurements that probe the correlations among a large number of particles. For example, randomized measurement techniques [24–27] provide an effective way to characterize global properties from measurements performed locally on individual particles, but generally require information about the correlations among a large number of local measurements. Since estimating multiparticle correlations becomes difficult when the system size scales up, it would be desirable to have a way to learn global properties from data collected only from a small number of neighboring sites. So far, the characterization

of many-body quantum states from short-range correlations has been investigated for the purpose of quantum state tomography [28–31]. For large quantum systems, however, a full tomography becomes challenging, and efficient methods for learning quantum properties from short-range correlations are still missing.

In this paper, we develop a neural network model that can predict various quantum properties of many-body quantum states from short-range correlations. Our model utilizes the technique of multi-task learning [32] to generate concise state representations that integrate diverse types of information. In particular, the model can integrate information obtained from few-body measurements into a representation of the overall quantum state, in a way that is reminiscent of the quantum marginal problem [33–35]. The state representations produced by our model are then used to learn new physical properties that were not seen during the training, including global properties such as string order parameters and many-body topological invariants [23].

For ground states with short-range correlations, we find that our model accurately predicts nonlocal features using only measurements on a few nearby particles. With respect to traditional, single-task neural networks, our model achieves more precise predictions with comparable amounts of input data, and enables a direct unsupervised classification of symmetry protected topological (SPT) phases that could not be distinguished in the single-task approach. In addition, we find that, after the training is completed, the model can be applied to quantum states and Hamiltonians outside the original training set, and even to quantum systems of higher dimension. This strong performance on out-of-distribution states suggests that our multi-task network could be used

* yzhu2@cs.hku.hk; Ya-Dong Wu and Yan Zhu contribute equally

† giulio@cs.hku.hk

as a tool to explore the next frontier of intermediate-scale quantum systems.

II. RESULTS

Multi-task framework for quantum properties.

Consider the scenario where an experimenter has access to multiple copies of an unknown quantum state ρ_θ , characterized by some physical parameters θ . For example, ρ_θ could be a ground state of many-body local Hamiltonian depending on θ . The experimenter's goal is to predict a set of properties of the quantum state, such as the expectation values of some observables, or some nonlinear functions, such as the von Neumann entropy. The experimenter is able to perform a restricted set of quantum measurements, denoted by \mathcal{M} . Each measurement $M \in \mathcal{M}$ is described by a positive operator-valued measure (POVM) $M = (M_j)$, where the index j labels the measurement outcome, each M_j is a positive operator acting on the system's Hilbert space, and the normalization condition $\sum_j M_j = I$ is satisfied. In general, the measurement set \mathcal{M} may not be informationally complete. For multipartite systems, we will typically take \mathcal{M} to consist of local measurements performed on a small number of neighboring systems.

To collect data, the experimenter randomly picks a subset of measurements $\mathcal{S} \subset \mathcal{M}$, and performs them on different copies of the state ρ_θ . We will denote by s the number of measurements in \mathcal{S} , and by $M_i := (M_{ij})$ the i -th POVM in \mathcal{S} . For simplicity, if not specified otherwise, we assume that each measurement in \mathcal{S} is repeated sufficiently many times that the experimenter can reliably estimate the outcome distribution $\mathbf{d}_i := (d_{ij})$, where $d_{ij} := \text{tr}(\rho M_{ij})$.

The experimenter's goal is to predict multiple quantum properties of ρ_θ using the outcome distributions $(\mathbf{d}_i)_{i=1}^s$. This task is achieved by a neural network that consists of an encoder and multiple decoders, where the encoder \mathcal{E} produces a representation of quantum states and the k -th decoder \mathcal{D}_k produces a prediction of the k -th property of interest. Due to their roles, the encoder and decoders are also known as representation and prediction networks, respectively.

The input of the representation network \mathcal{E} is the outcome distribution \mathbf{d}_i , together with a parametrization of the corresponding measurement M_i , hereafter denoted by \mathbf{m}_i . From the pair of data $(\mathbf{d}_i, \mathbf{m}_i)$, the network produces a state representation $\mathbf{r}_i := \mathcal{E}(\mathbf{d}_i, \mathbf{m}_i)$. To combine the state representations arising from different measurements in \mathcal{S} , the network computes the average $\mathbf{r} := \frac{1}{s} \sum_{i=1}^s \mathbf{r}_i$. At this point, the vector \mathbf{r} can be viewed as a representation of the unknown quantum state ρ .

Each prediction network \mathcal{D}_k is dedicated to a different property of the quantum state. In the case of multipartite quantum systems, we include the option of evaluating the property on a subsystem, specified by a parameter

q . We denote by $f_{k,q}(\rho_\theta)$ the correct value of the k -th property of subsystem q when the total system is in the state ρ_θ . Upon receiving the state representation \mathbf{r} and the subsystem specification q , the prediction network produces an estimate $\mathcal{D}_k(\mathbf{r}, q)$ of the value $f_{k,q}(\rho)$.

The representation network and all the prediction networks are trained jointly, with the goal of minimizing the prediction error on a set of fiducial states. The fiducial states are chosen by randomly sampling a set of physical parameters $(\theta_l)_{l=1}^L$. For each fiducial state ρ_{θ_l} , we independently sample a set of measurements \mathcal{S}_l and calculate the outcome distributions for each measurement in the set \mathcal{S}_l . We randomly choose a subset of properties \mathcal{K}_l for each ρ_{θ_l} , where each property $k \in \mathcal{K}_l$ corresponds to a set of subsystems \mathcal{Q}_k , and then calculate the correct values of the quantum properties $\{f_{k,q}(\rho_{\theta_l})\}$ for all properties $k \in \mathcal{K}_l$ associated with subsystems $q \in \mathcal{Q}_k$. The training data may be either classically simulated or gathered by actual measurements on the set of fiducial states, or it could also be obtained by any combination of these two approaches.

During the training, we do not provide the model with any information about the physical parameters θ_l or about the functions $f_{k,q}$. Instead, the internal parameters of the neural networks are jointly optimized in order to minimize the estimation errors $|\mathcal{D}_k(1/s \sum_{i=1}^s \mathcal{E}(\{\mathbf{d}_i, \mathbf{m}_i\}), q) - f_{k,q}(\rho_\theta)|$ summed over all the fiducial states, all chosen properties, and all chosen subsystems.

After the training is concluded, our model can be used for predicting quantum properties, either within the set of properties seen during training or outside this set. The requested properties are predicted on a new, unknown state ρ_θ , and even out-of-distribution state ρ that has a structural similarity with the states in the original distribution, e.g., a ground state of the same type of Hamiltonian, but for a quantum system with a larger number of particles.

The high-level structure of our model is illustrated in Figure 1, while the details of the neural networks are presented in Methods.

Learning ground states of Cluster-Ising model

We first test the performance of our model on a relatively small system of $N = 9$ qubits whose properties can be explicitly calculated. For the state family, we take the ground states of one-dimensional cluster-Ising model [36]

$$H_{\text{CI}} = - \sum_{i=1}^{N-2} \sigma_i^z \sigma_{i+1}^x \sigma_{i+2}^z - h_1 \sum_{i=1}^N \sigma_i^x - h_2 \sum_{i=1}^{N-1} \sigma_i^x \sigma_{i+1}^x. \quad (1)$$

The ground state falls in one of three phases, depending on the values of the parameters (h_1, h_2) . The three phases are: the SPT phase, the paramagnetic phase, and the antiferromagnetic phase. SPT phase

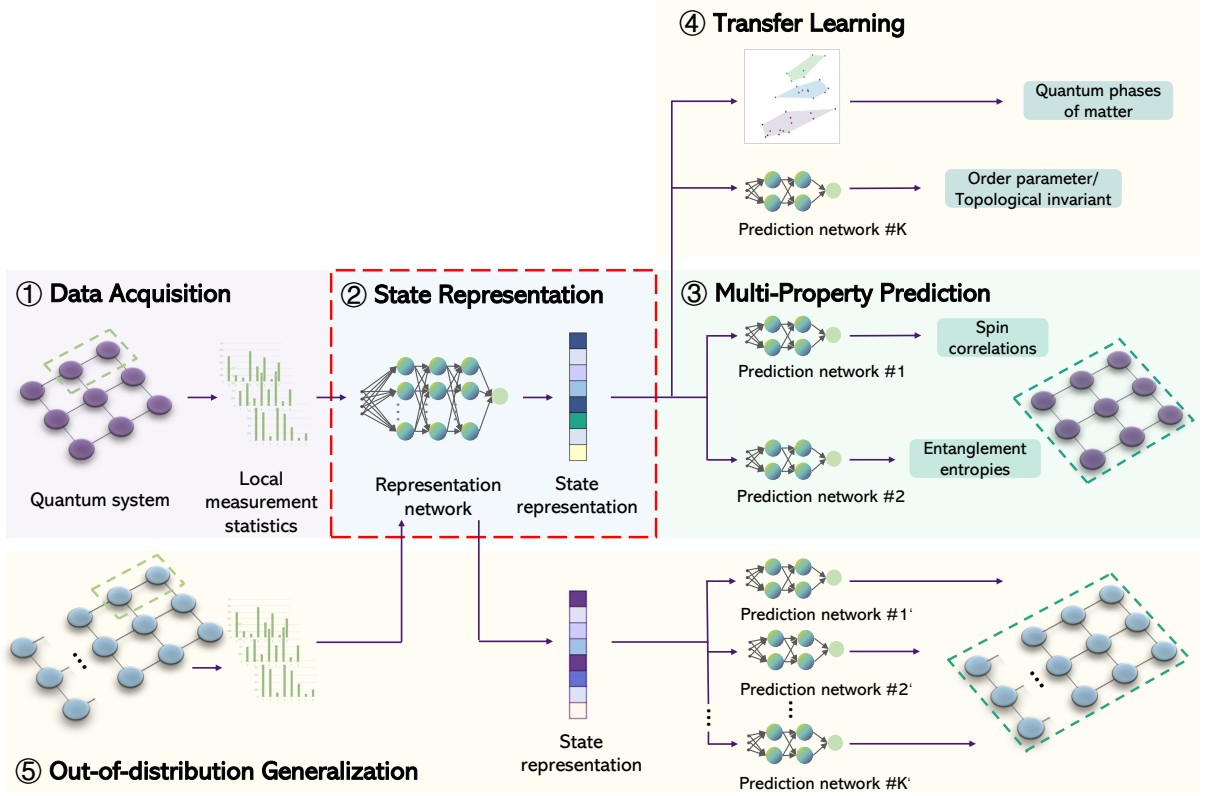


Figure 1. Flowchart of our multi-task neural network. In the data acquisition phase (1), the experimenter performs short-range local measurements on the system of interest. The resulting data is used to produce a concise representation of the quantum state (2). The state representation is then fed into a set of prediction networks, each of which generates predictions for a given type of quantum property (3). After the state representation network and prediction networks are jointly trained, the state representations are employed in new tasks, such as unsupervised classification of quantum phases of matter, or prediction of order parameters and topological invariants (4). Once trained, the overall model can generally be applied to out-of-distribution quantum states and higher-dimensional quantum systems (5).

can be distinguished from two other phases by measuring the string order parameter [37, 38] $\langle \tilde{S} \rangle := \langle \sigma_1^z \sigma_2^x \sigma_4^x \dots \sigma_{N-3}^x \sigma_{N-1}^x \sigma_N^z \rangle$, which is a global property involving $(N+3)/2$ qubits.

We test our network model on the ground states corresponding to a 64×64 square grid in the parameter region $(h_1, h_2) \in [0, 1.6] \times [-1.6, 1.6]$. For the set of accessible measurements \mathcal{M} , we take all possible three-nearest-neighbour Pauli measurements, corresponding to the observables $\sigma_i^\alpha \otimes \sigma_{i+1}^\beta \otimes \sigma_{i+2}^\gamma$, where $i \in \{1, 2, \dots, N-2\}$ and $\alpha, \beta, \gamma \in \{x, y, z\}$.

For the prediction tasks, we consider two properties: (A1) the two-point correlation function $\mathcal{C}_{1j}^\alpha := \langle \sigma_1^\alpha \sigma_j^\alpha \rangle_\rho$, where $1 < j \leq N$ and $\alpha = x, z$; (A2) the Rényi entanglement entropy of order two $S_A := -\log_2(\text{tr} \rho_A^2)$ for subsystem $A = [1, 2, \dots, i]$, where $1 \leq i < N$. Both properties (A1) and (A2) can be either numerically evaluated, or experimentally estimated by preparing the appropriate quantum state and performing randomized measurements [26].

We train our neural network with respect to the fiducial ground states corresponding to 300 randomly cho-

sen points from our 4096-element grid. For each fiducial state, we provide the neural network with the outcome distributions of $s = 50$ measurements, randomly chosen from the 243 measurements in \mathcal{M} . Half of these fiducial states randomly chosen from the whole set are labeled by the values of property (A1) and the other half are labeled by property (A2). After training is concluded, we apply our trained model to predicting properties (A1)-(A2) for all remaining ground states corresponding to points on the grid. For each test state, the representation network is provided with the outcome distributions on $s = 50$ measurement settings randomly chosen from \mathcal{M} .

Figure 2a illustrates the coefficient of determination (R^2), averaged over all test states, for each type of property. Notably, all the values of R^2 observed in our experiments are above 0.95. Our network makes accurate predictions even near the boundary between the SPT phase and paramagnetic phase, in spite of the fact that phase transitions typically make it more difficult to capture the ground state properties from limited measurement data. For a ground state close to the boundary, marked by a star in the phase diagram (Figure 3d), the predictions of the entanglement entropy S_A and spin correlation \mathcal{C}_{1j}^z

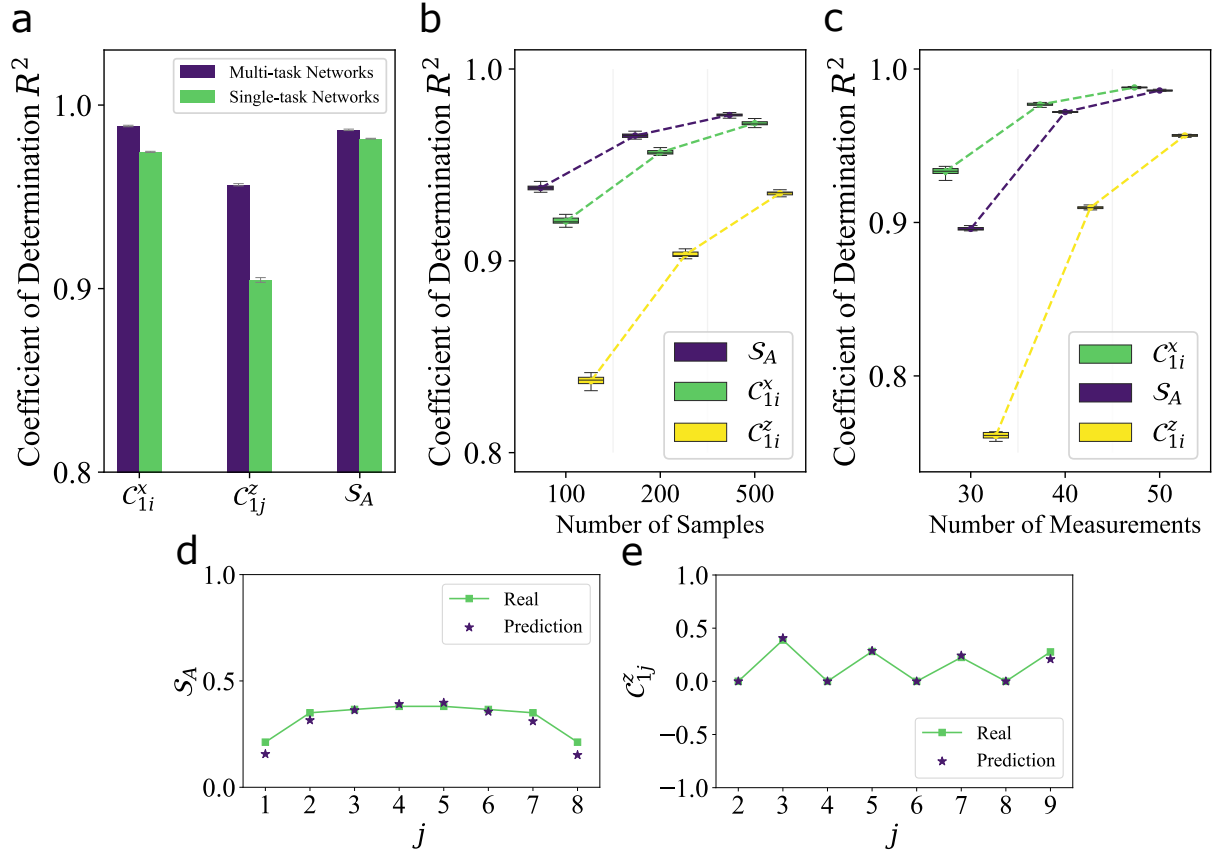


Figure 2. Predicting properties of ground states of cluster-Ising model. Subfigure **a** compares the prediction accuracy between our multi-task model and single-task models for predicting two-point correlation functions C_{1j}^x and C_{1j}^z , and entanglement entropy S_A . Subfigures **b** and **c** show how the number of samples for each measurement and the number of measurements affect the coefficient of determination for the predictions of S_A , C_{1j}^x and C_{1j}^z , respectively. Subfigures **d** and **e** show the predictions of S_A and C_{1j}^z for a ground state near phase transition marked by a red star in Subfigure **3d**.

are close to the corresponding ground truths, as shown in Figures **2d** and **2e**, respectively.

In general, the accuracy of the predictions depends on the number of samplings for each measurement as well as the number of measurement settings. For our experiments, the dependence is illustrated in Figures **2b** and **2c**.

To examine whether our multi-task neural network model enhances the prediction accuracy compared to single-task networks, we perform ablation experiments [39]. We train three individual single-task neural networks as our baseline models, each of which predicts spin correlations in Pauli-x axis, spin correlations in Pauli-z axis, and entanglement entropies, respectively. For each single-task neural network, the training provides the network with the corresponding properties for the 300 fiducial ground states, without providing any information about the other properties. After the training is concluded, we apply each single-task neural network to predict the corresponding properties on all the test states and use their predictions as baselines to benchmark the performance of our multi-task neural network. Figure **2a** compares the values of R^2 for the predictions

of our multi-task neural model with those of the single-task counterparts. The results demonstrate that learning multiple physical properties simultaneously enhances the prediction of each individual property.

Transfer learning to new tasks

We now show that the state representations produced by the encoder can be used to perform new tasks that were not encountered during the training phase. In particular, we show that state representations can be used to distinguish between the phases of matter associated to different values of the Hamiltonian parameters in an unsupervised manner. To this purpose, we project the representations of all the test states onto a two-dimensional (2D) plane using the t-distributed stochastic neighbour embedding (t-SNE) algorithm.

The results are shown in Figure **3a**. Every data point shows the exact value of the string order parameter, which distinguishes between the SPT phase and the other two phases. Quite strikingly, we find that the disposition

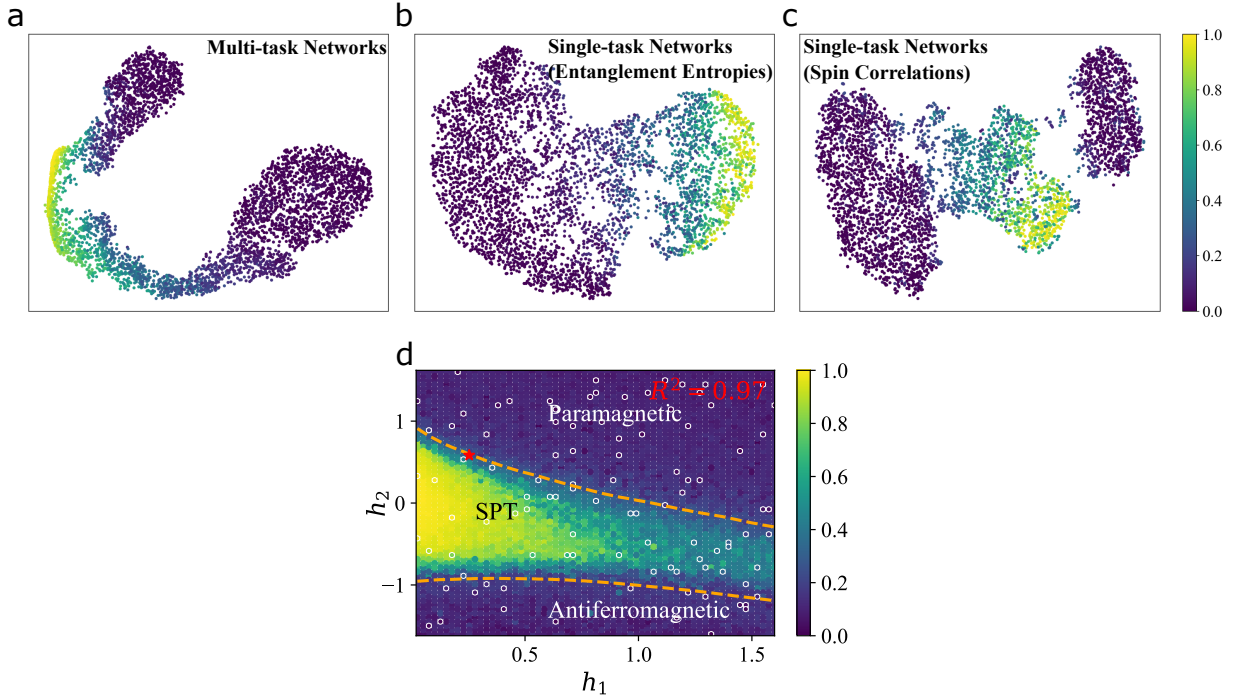


Figure 3. Transfer learning to predict properties of the ground states of the cluster-Ising model. Subfigures **a**, **b** and **c** illustrate the 2D projection of the state representations obtained with the t-SNE algorithm, where the color of each data point indicates the true value of the string order parameter $\langle \tilde{S} \rangle$ of the corresponding ground state. Subfigure **a** corresponds to the state representations produced for jointly predicting spin correlations and entanglement entropy. Subfigures **b** and **c** correspond to the state representations produced for separately predicting entanglement entropy and spin correlations, respectively. Subfigure **d** shows the predictions of $\langle \tilde{S} \rangle$ for the ground states corresponding to a 64×64 grid in parameter space, together with the true values of $\langle \tilde{S} \rangle$ for 100 randomly chosen states indicated by white circles, where the dashed curves are the phase boundaries between SPT phase and the other two phases.

of the points in the 2D representation matches the values of the string order parameter, even though no information about the string order parameters was provided during the training, and even though the string order is a global property, while the measurement data provided to the network came from a small number of neighboring sites.

A natural question is whether the accurate classification of phases of matter observed above is a consequence of the multi-task nature of our model. To shed light into this question, we compare the results of our multi-task network with those of single-task neural networks, feeding the state representations generated by these networks into the t-SNE algorithm to produce a 2D representation. The pattern of the projected state representations in Figure 3b indicates that when trained only with the values of entanglement entropies, the neural network cannot distinguish between the paramagnetic phase and the antiferromagnetic phase. Interestingly, a single-task network trained only on the spin correlations can still distinguish the SPT phase from the other two phases, as shown in Figure 3c. However, in the next section we see that applying random local gates induces errors in the single-task network, while the multi-task network still achieves a correct classification of the different phases.

Quantitatively, the values of the string order parameter can be extracted from the state representations using another neural network \mathcal{N} . To train this network, we randomly pick 100 reference states $\{\sigma_i\}$ out of the 300 fiducial states and minimize the error $\sum_{i=1}^{100} |\mathcal{N}(\mathbf{r}_{\sigma_i}) - \langle \tilde{S} \rangle_{\sigma_i}|$. Then, we use the trained neural network \mathcal{N} to produce the prediction $\mathcal{N}(\mathbf{r}_\rho)$ of $\langle \tilde{S} \rangle_\rho$ for every other state ρ . The prediction for each ground state is shown in the phase diagram (Figure 3d), where the 100 reference states are marked by white circles. The predictions are close to the true values of string order parameters in Figure 5c. It is important to stress that, while the network \mathcal{N} was trained on values of the string order parameter, the representation network \mathcal{E} was not provided any information about this parameter. Note also that the values of the Hamiltonian parameters (h_1, h_2) are just provided in the figure for the purpose of visualization: in fact, no information about the Hamiltonian parameters was provided to the network during training or test. In Supplementary Note 6, we show that our neural network model trained for predicting entanglement entropy and spin correlations can also be transferred to other ground-state properties of the cluster-Ising model.

Generalization to out-of-distribution states

In the previous sections, we assumed that both the training and the testing states were randomly sampled from a set of ground states of the cluster-Ising model (1). In this subsection, we explore how a model trained on a given set of quantum states can generalize to states outside the original set in an unsupervised or weakly supervised manner.

Our first finding is that our model, trained on the ground states of the cluster-Ising model, can effectively cluster general quantum states in the SPT phase and the trivial phase (respecting the symmetry of bit flips at even/odd sites), without further training. Random quantum states in SPT (trivial) phase can be prepared by applying short-range symmetry-respecting local random quantum gates on a cluster state in the SPT phase (a product state $|+\rangle^{\otimes N}$ in the paramagnetic phase). For these random quantum states, we follow the same measurement strategy adopted before, feed the measurement data into our trained representation network, and use t-SNE to project the state representations onto a 2D plane.

When the quantum circuit consists of a layer of translation-invariant next-nearest neighbour symmetry-respecting random gates, our model successfully classifies the output states into their respective SPT phase and trivial phase in both cases, as shown by Figure 4a. In contrast, feeding the same measurement data into the representation network trained only on spin correlations fails to produce two distinct clusters via t-SNE, as shown by Figure 4b. While this neural network successfully classifies different phases for the cluster-Ising model, random local quantum gates confuse it. This failure is consistent with the recent observation that extracting linear functions of a quantum state is insufficient for classifying arbitrary states within SPT phase and trivial phase [40].

We then prepare more complex states by applying two layers of translation-invariant random gates consisting of both nearest neighbour and next-nearest neighbour gates preserving the symmetry onto the initial states. The results in Figure 4c show that the state representations of these two phases remain different, but the boundary between them in the representation space is less clearly identified. Whereas, the neural network trained only on spin correlations fails to classify these two phases, as shown by Figure 4d.

Finally, we demonstrate that our neural model, trained on the cluster-Ising model, can adapt to learn the ground states of a new, perturbed Hamiltonian [41]

$$H_{\text{pcI}} = H_{\text{cl}} + h_3 \sum_{i=1}^{N-1} \sigma_i^z \sigma_{i+1}^z. \quad (2)$$

This perturbation breaks the original symmetry, shifts the boundary of the cluster phase, and introduces a new phase of matter. In spite of these substantial changes, Figure 5a shows that our model, trained on the unperturbed cluster-Ising model, successfully identifies the dif-

ferent phases, including the new phase from the perturbation. Moreover, using just 10 randomly chosen additional reference states (marked by white circles in Figure 5b), the original prediction network can be adjusted to predict the values of $\langle \tilde{S} \rangle$ from state representations. As shown in Figure 5b, the predicted values closely match the ground truths in Figure 5c, achieving a coefficient of determination of up to 0.956 between the predictions and the ground truths.

Learning ground states of XXZ model

We now apply our model to a larger quantum system, consisting of 50 qubits in ground states of the bond-alternating XXZ model [42]

$$H = J \sum_{i=1}^{N/2} (\sigma_{2i-1}^x \sigma_{2i}^x + \sigma_{2i-1}^y \sigma_{2i}^y + \delta \sigma_{2i-1}^z \sigma_{2i}^z) + J' \sum_{i=1}^{N/2-1} (\sigma_{2i}^x \sigma_{2i+1}^x + \sigma_{2i}^y \sigma_{2i+1}^y + \delta \sigma_{2i}^z \sigma_{2i+1}^z), \quad (3)$$

where J and J' are the alternating values of the nearest-neighbor spin couplings. We consider a set of ground states corresponding to a 21×21 square grid in the parameter region $(J/J', \delta) \in (0, 3) \times (0, 4)$. Depending on the ratio of J/J' and the strength of δ , the corresponding ground state falls into one of three possible phases: trivial SPT phase, topological SPT phase, and symmetry broken phase.

Unlike the SPT phases of cluster-Ising model, the SPT phases of bond-alternating XXZ model cannot be detected by any string order parameter. Both SPT phases are protected by bond-center inversion symmetry, and detecting them requires a many-body topological invariant, called the partial reflection topological invariant [42] and denoted by

$$\mathcal{Z}_R := \frac{\text{tr}(\rho_I \mathcal{R}_I)}{\sqrt{[\text{tr}(\rho_{I_1}^2) + \text{tr}(\rho_{I_2}^2)]/2}}. \quad (4)$$

Here, \mathcal{R}_I is the swap operation on subsystem $I := I_1 \cup I_2$ with respect to the center of the spin chain, and $I_1 = [N/2 - 5, N/2 - 4, \dots, N/2]$ and $I_2 = [N/2 + 1, N/2 + 2, \dots, N/2 + 6]$ are two subsystems with six qubits.

For the set of possible measurements \mathcal{M} , we take all possible three-nearest-neighbour Pauli projective measurements, as we did earlier in the cluster-Ising model. For the prediction tasks, we consider two types of quantum properties: (B1) nearest-neighbour spin correlations $\mathcal{C}_{i,i+1}^\beta := \langle \sigma_i^\beta \sigma_{i+1}^\beta \rangle$ ($1 \leq i \leq N - 1$), where $\beta = x, z$; (B2) order-two Rényi mutual information $I_{A:B}$, where A and B are both 4-qubit subsystems: either $A_1 = [22 : 25]$, $B_1 = [26 : 29]$ or $A_2 = [21 : 24]$, $B_2 = [25 : 28]$.

We train our neural network with respect to the fiducial ground states corresponding to 80 pairs of $(J/J', \delta)$,

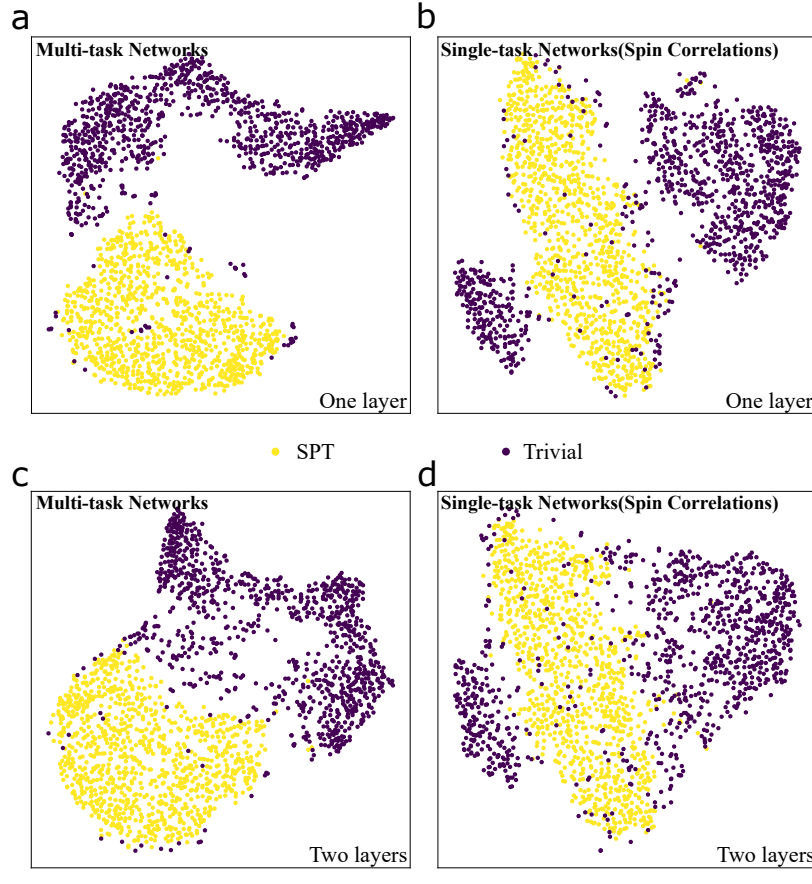


Figure 4. 2D projections of state representations for those states prepared by shallow random symmetric quantum circuits. Subfigures **a** and **b** correspond quantum states in the SPT and the trivial phases prepared by one layer of random quantum gates, and Subfigures **c** and **d** correspond quantum states in the SPT and the trivial phases prepared by two layers of random quantum gates. Subfigures **a** and **c** illustrate state representations produced by our multi-task neural network. Subfigures **b** and **d** illustrate state representations produced by the neural network trained only on spin correlations.

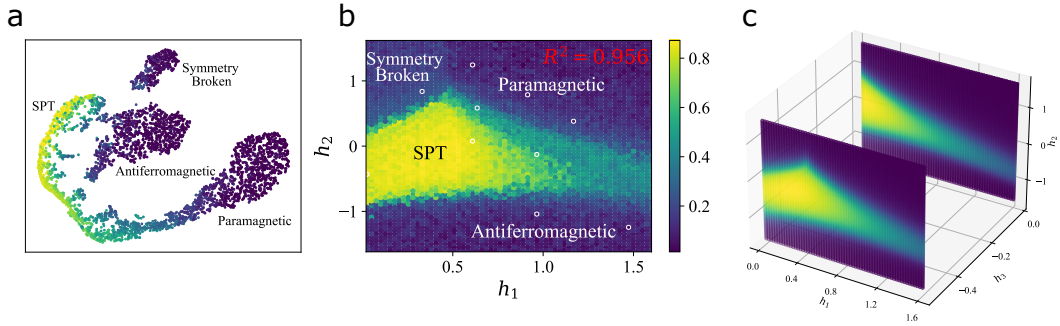


Figure 5. Prediction of properties of ground states of a perturbed Hamiltonian. Subfigure **a** illustrates the 2D projections of state representations for the ground states of the perturbed Hamiltonian, together with their true values of $\langle \tilde{S} \rangle$. Subfigure **b** illustrates the predictions of $\langle \tilde{S} \rangle$ using our adjusted neural network for the perturbed model. Subfigure **c** show the true values of string order parameters $\langle \tilde{S} \rangle$ for both the original model (1) and the perturbed model (2).

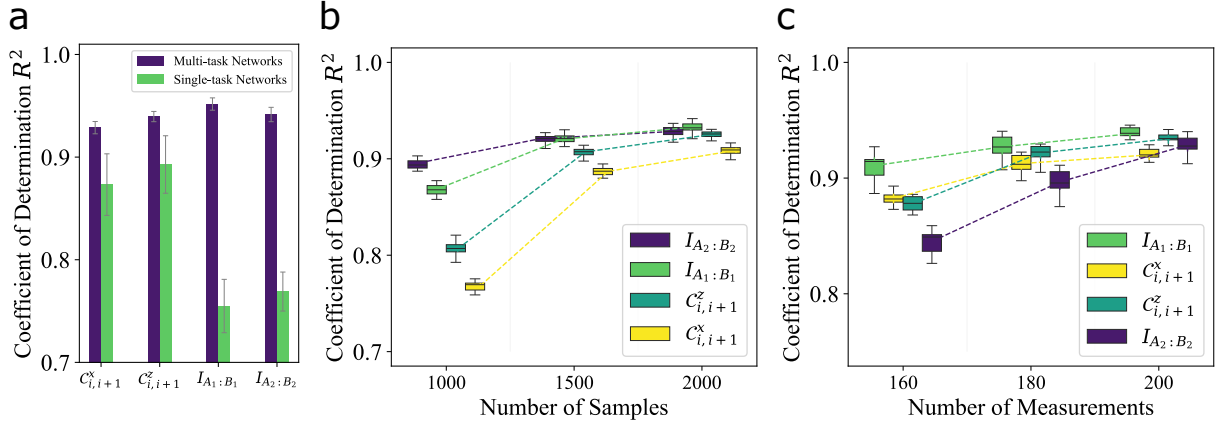


Figure 6. Predicting properties of 50 qubit ground states of bond-alternating XXZ model. Subfigure **a** compares the prediction accuracy between our multi-task model and single-task models for predicting spin correlations $C_{i,i+1}^x$ and $C_{i,i+1}^z$, as well as Rényi mutual information $I_{A:B}$. Subfigure **b** and **c** show how the number of samples for each measurement and the number of measurements affect the coefficient of determination for the predictions of all the properties.

randomly sampled from the 441-element grid. For each fiducial state, we provide the neural network with the probability distributions corresponding to $s = 200$ measurements randomly chosen from the 1350 measurements in \mathcal{M} . Half of the fiducial states randomly chosen from the entire set are labeled by the property of (B1), while the other half are labeled by the property of (B2). After the training is concluded, we use our trained model to predict both properties (B1) and (B2) for all the ground states in the grid.

Figure 6a demonstrates the strong predictive performance of our model, where the values of R^2 are above 0.92 for all properties averaged over test states. We benchmark the performances of our multi-task neural network with the predictions of single-task counterparts. Here each single-task neural network, the size of which is same as the multi-task network, aims at predicting one single physical property and is trained using the same set of measurement data of 80 fiducial states together with one of their properties: $C_{i,i+1}^x$, $C_{i,i+1}^z$, $I_{A_1:B_1}$ and $I_{A_2:B_2}$. Figure 6a compares the coefficients of determination for the predictions of both our multi-task neural network and the single-task neural networks, where each experiment is repeated multiple times over different sets of $s = 200$ measurements randomly chosen from \mathcal{M} . The results indicate that our multi-task neural model not only achieves higher accuracy in the predictions of all properties, but also is much more robust to different choices of quantum measurements. As in the case of the cluster-Ising model, we also study how the number of quantum measurements s and the number of samplings for each quantum measurement affect the prediction accuracy of our neural network model, as shown by Figures 6b and 6c. Additionally, we test how the size of the quantum system affects the prediction accuracy given the same amount of local measurement data (see Supplementary Note 7).

To highlight the importance of our representation neu-

ral network for good prediction accuracy, we replaced it with principal component analysis (PCA) and trained individual prediction neural networks with PCA-generated representations as input. This simplification resulted in a complete failure to predict any (B1) or (B2) properties (see Supplementary Note 5). This reveals that PCA cannot extract the essential information of quantum states from their limited measurement data, a task successfully accomplished by our trained representation network.

We show that, even in the larger-scale example considered in this section, the state representations obtained through multi-task training contain information about the quantum phases of matter. In Figure 7a, we show the 2D-projection of the state representations. The data points corresponding to ground states in the topological SPT phase, the trivial SPT phase and the symmetry broken phase appear to be clearly separated into three clusters, while the latter two connected by a few data points corresponding to ground states across the phase boundary. A few points, corresponding to ground states near phase boundaries of the topological SPT phase, are incorrectly clustered by the t-SNE algorithm. The origin of the problem is that the correlation length of ground states near phase boundary becomes longer, and therefore the measurement statistics on nearest-neighbour-three qubit subsystems cannot capture sufficient information for predicting the correct phase of matter.

We further examine if the single-task neural networks above can correctly classify the three different phases of matter. We project the state representations produced by each single-task neural network onto 2D planes by the t-SNE algorithm, as shown by Figures 7b and 7c. The pattern of projected representations in Figure 7b implies that when trained only with the values of spin correlations, the neural network cannot distinguish the topological SPT phase from the trivial SPT phase. The pattern in Figure 7c indicates that when trained solely

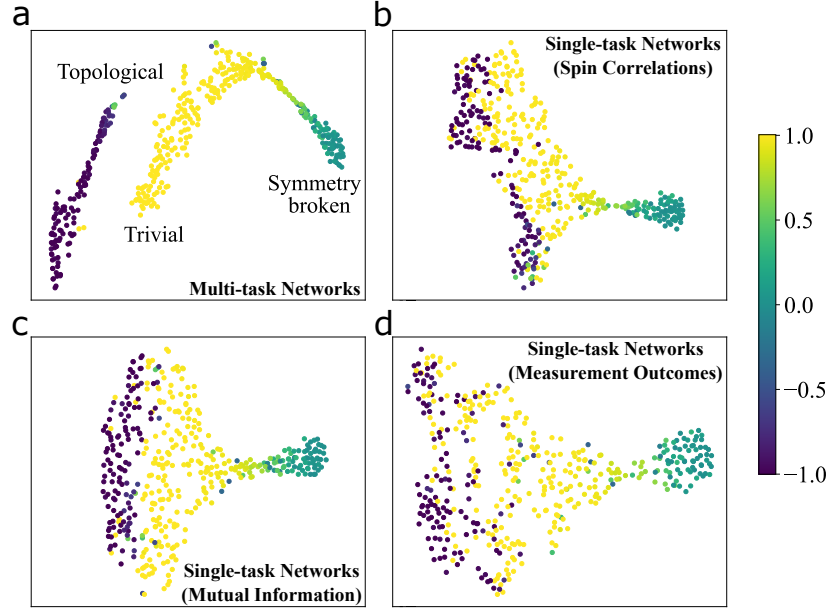


Figure 7. 2D projections of the state representations for bond-alternating XXZ model obtained with the t-SNE algorithm. The color of each data point indicates the true value of many-body topological invariant \mathcal{Z}_R of the corresponding ground state. Subfigure **a** corresponds to the state representations produced for predicting both spin correlations and mutual information. Whereas, Subfigures **b**, **c** and **d** correspond to the state representations produced for predicting spin correlations, mutual information and measurement outcome distributions respectively.

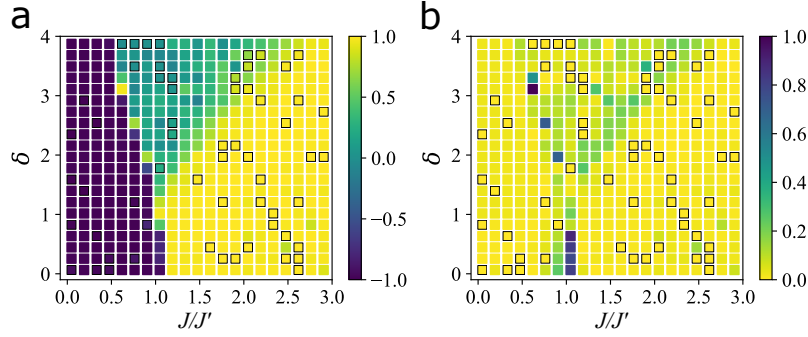


Figure 8. Predictions of many-body topological invariants. Subfigure **a** shows the predictions of \mathcal{Z}_R for the ground states corresponding to all pairs of parameters $(J/J', \delta)$ together with the true values of 60 reference states marked by grey squares. Subfigure **b** shows the absolute values of the differences between predictions and the ground truths.

with mutual information, the performance of clustering is slightly improved, but still cannot explicitly classify these two SPT phases. We also project the state representations produced by the neural network for predicting measurement outcome statistics [3] onto a 2D plane. The resulting pattern, shown in Figure 7d, shows that the topological SPT phase and the trivial SPT phase cannot be correctly classified either. These observations indicate that a multi-task approach, including both the properties of mutual information and spin correlations, is necessary to capture the difference between the topological SPT phase and the trivial SPT phase.

The emergence of clusters related to different phases of matter suggests that the state representation produced

by our network also contains quantitative information about the topological invariant \mathcal{Z}_R . To extract this information, we use an additional neural network, which maps the state representation into a prediction of \mathcal{Z}_R . We train this additional network by randomly selecting 60 reference states (marked by grey squares in Figure 8) out of the set of 441 fiducial states, and by minimizing the prediction error on the reference states. The predictions together with 60 exact values of the reference states are shown in Figure 8a. The absolute values of the differences between the predictions and ground truths are shown in Figure 8b. The predictions are close to the ground truths, except for the ground states near the phase boundaries, especially the boundary of topological

SPT phase. The mismatch at the phase boundaries corresponds to the state representations incorrectly clustered in Figure 7a, suggesting our network struggles to learn long-range correlations at phase boundaries.

Generalization to quantum systems of larger size

We now show that our model is capable of extracting features that are transferable across different system sizes. To this purpose, we use a training dataset generated from 10-qubit ground states of the bond-alternating XXZ model (3) and then we use the trained network to generate state representations from the local measurement data of each 50-qubit ground state of (3).

Figure 9a shows that inputting the state representations into the t-SNE algorithm still gives rise to clusters according to the three distinct phases of matter. This observation suggests that the neural network can effectively classify different phases of the bond-alternating XXZ model, irrespective of the system size. In addition to clustering larger quantum states, the representation network also facilitates the prediction of quantum properties in the larger system. To demonstrate this capability, we employ 40 reference ground states of the 50-qubit bond-alternating XXZ model, which are only half size of the training dataset used for 10-qubit system, to train two prediction networks: one for spin correlations and the other for mutual information. Figure 9b shows the coefficients of determination for each prediction, which exhibit values around 0.9 or above. Figure 9b also shows the impact of inaccurate labelling of the ground states on our model. In the reported experiments, we assumed that 10% of the labels in the training dataset corresponding to 40 reference states are randomly incorrect, while the remaining 90% are accurate. Without any mitigation, we observe that the errors substantially impacts the accuracy of our predictions. On the other hand, employing a technique of noise mitigation during the training of prediction networks (see Supplementary Note 7) can effectively reduce the impact of the incorrect labels.

III. DISCUSSION

The use of short-range local measurements is a key distinction between our work and prior approaches approaches using randomized measurements [24, 26, 40, 43]. Rather than measuring all spins together, we employ randomized Pauli measurements on small groups of neighboring sites. This feature is appealing for practical applications, as measuring correlations among large numbers of sites is generally challenging. In Supplementary Note 5, we show that classical shadow estimation cannot be directly adapted to the scenario where only short-range local measurements are available. On the other hand, the restriction to short-range local measurements implies that the applicability of our method is limited to many-

body quantum states with a constant correlation length, such as the ground state within an SPT phase.

A crucial aspect of our neural network model is its ability to generate a latent state representation that integrates different pieces of information, corresponding to multiple physical properties. Remarkably, the state representations appear to capture information about properties beyond those encountered in training. This feature allows for unsupervised classification of phases of matter, applicable not only to in-distribution Hamiltonian ground states but also to out-of-distribution quantum states, like those produced by random circuits. The model also appears to be able to generalize from smaller to larger quantum systems, which makes it an effective tool for exploring intermediate-scale quantum systems.

For new quantum systems, whose true phase diagrams is still unknown, discovering phase diagrams in an unsupervised manner is a major challenge. This challenge can potentially be addressed by combining our neural network with consistency-checking, similar to the approach in Ref. [19]. The idea is to start with an initial, potentially inaccurate, phase diagram ansatz constructed from limited prior knowledge, for instance, the results of clustering. Then, one can randomly select a set of reference states, labeling them according to the ansatz phases. Based on these labels, a separate neural network is trained to predict phases. Finally, the ansatz can be revised based on the deviation with the network's prediction, and the procedure can be iterated until it converges to a stable ansatz. In Supplementary Note 8, we provide examples of this approach, leaving the development of a full algorithm for autonomous discovery of phase diagram as future work.

IV. METHODS

Data generation. Here we illustrate the procedures for generating training and test datasets. For the one-dimensional cluster-Ising model, we obtain measurement statistics and values for various properties in both the training and test datasets through direct calculations, leveraging the ground states solved by exact algorithms. In the case of the one-dimensional bond-alternating XXZ model, we first obtain approximate ground states represented by matrix product states [44, 45] using the density-matrix renormalization group (DMRG) [46] algorithm. Subsequently, we compute the measurement statistics and properties by contracting the tensor networks. For the noisy measurement statistics because of finite sampling, we generate them by sampling from the actual probability distribution of measurement outcomes. More details are provided in Supplementary Note 1.

Representation Network. The representation network operates on pairs of measurement outcome distributions and the parameterization of their corresponding measurements, denoted as $(\mathbf{d}_i, \mathbf{m}_i)_{i=1}^m$ associated with a state ρ . This network primarily consists of three multilayer per-

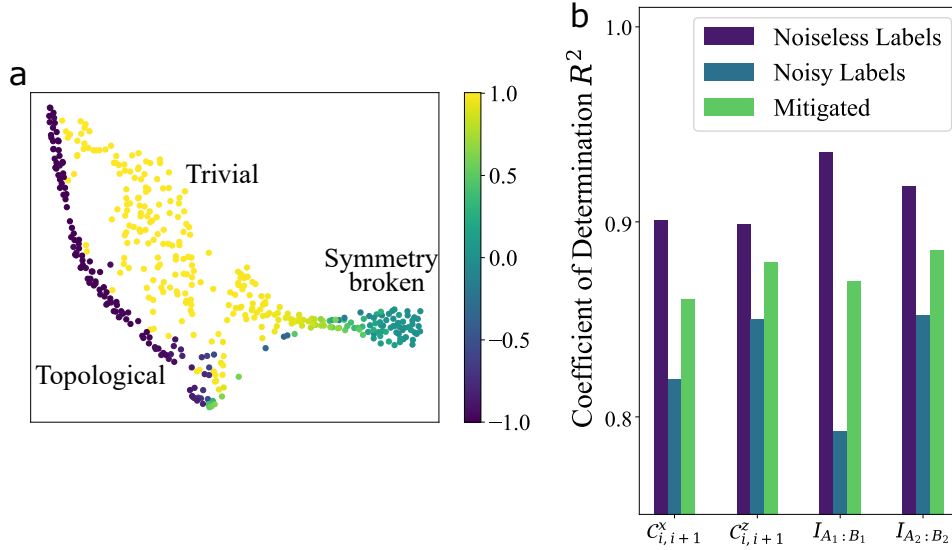


Figure 9. Predictions of properties of 50-qubit systems made by a neural network trained over the data of 10-qubit systems. Subfigure **a** shows the 2D projections of state representations via t-SNE algorithm. Subfigure **b** shows the coefficient of determination for the predictions of properties using noiseless training labels and noisy training labels, as well as the predictions after error mitigation.

ceptrons (MLPs) [47]. The first MLP comprises a four-layer architecture that transforms the measurement outcome distribution into \mathbf{h}_i^d , whereas the second two-layer MLP maps the corresponding \mathbf{m}_i to \mathbf{h}_i^m :

$$\begin{aligned}\mathbf{h}_i^d &= \text{MLP}_1(\mathbf{d}_i), \\ \mathbf{h}_i^m &= \text{MLP}_2(\mathbf{m}_i).\end{aligned}$$

Next, we merge \mathbf{h}_i^d and \mathbf{h}_i^m , feeding them into another three-layer MLP to obtain a partial representation denoted as \mathbf{r}_i for the state:

$$\mathbf{r}_\rho^{(i)} = \text{MLP}_3([\mathbf{h}_i^d, \mathbf{h}_i^m]). \quad (5)$$

Following this, we aggregate all the \mathbf{r}_i representations through an average pooling layer to produce the complete state representation, denoted as \mathbf{r}_ρ :

$$\mathbf{r}_\rho = \frac{1}{s} \sum_{i=1}^s \mathbf{r}_i. \quad (6)$$

Alternatively, we can leverage a recurrent neural network equipped with gated recurrent units (GRUs) [48] to derive the comprehensive state representation from the set $\{\mathbf{r}_i\}_{i=1}^m$:

$$\begin{aligned}\mathbf{z}_i &= \text{sigmoid}(W_z \mathbf{r}_\rho^{(i)} + U_z \mathbf{r}_\rho^{(i-1)} + \mathbf{b}_z), \\ \hat{\mathbf{h}}_i &= \tanh(W_h \mathbf{r}_\rho^{(i)} + U_h (\mathbf{z}_i \odot \mathbf{h}_{i-1}) + \mathbf{b}_h), \\ \mathbf{h}_i &= (1 - \mathbf{z}_i) \odot \mathbf{h}_{i-1} + \mathbf{z}_i \odot \hat{\mathbf{h}}_i, \\ \mathbf{r}_\rho &= \mathbf{h}_m,\end{aligned}$$

where W, U, \mathbf{b} are trainable matrices and vectors. The architecture of the recurrent neural network offers a more flexible approach to generate the complete state representation; however, in our experiments, we did not observe significant advantages compared to the average pooling layer.

Reliability of Representations. The neural network can assess the reliability of each state representation by conducting contrastive analysis within the representation space. Figure 10 shows a measure of the reliability of each state representation, which falls in the region $[0, 1]$, for both the cluster-Ising model and the bond-alternating XXZ model. As this measure increases from 0 to 1, the reliability of the corresponding prediction strengthens, with values closer to 0 indicating low reliability and values closer to 1 indicating high reliability. Figure 10a indicates that the neural network exhibits lower confidence for the ground states in SPT phase than those in the other two phases, with the lowest confidence occurring near the phase boundaries. Figure 10b shows that the reliability of predictions for the ground states of the XXZ model in two SPT phases are higher than those in the symmetry broken phase, which is due to the imbalance of training data, and that the predictions for quantum states near the phase boundaries have the lowest reliability. Here, the reliability is associated with the distance between the state representation and its cluster center in the representation space. We adopt this definition based on the intuition that for a quantum state that the model should exhibit higher confidence for quantum states that cluster more easily.

Distance-based methods [49, 50] have proven effective in the task of Out-of-Distribution detection in classical machine learning. This task focuses on identifying in-

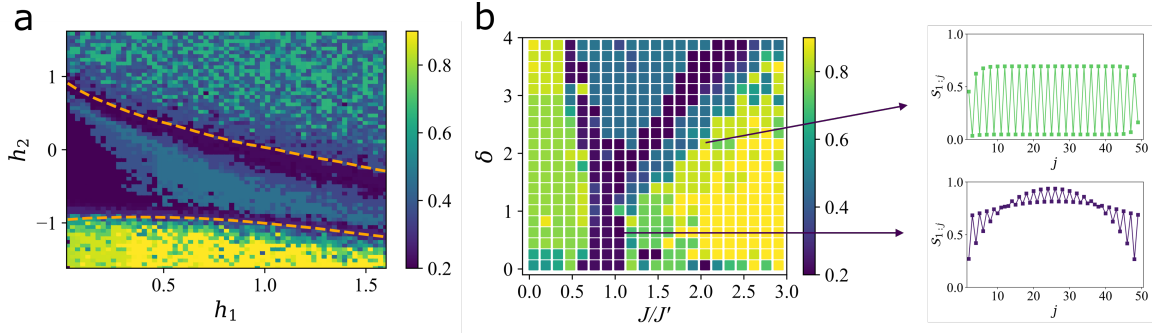


Figure 10. A measure of reliability of state representations. Subfigure **a** shows the reliability of the representation of each ground state of the cluster-Ising model. Subfigure **b** illustrates the reliability of the representation of each ground state of the bond-alternating XXZ model, together with the true subsystem entanglement entropy for two example states: one is near the phase boundary and the other is further away from the phase boundary.

stances that significantly deviate from the data distribution observed during training, thereby potentially compromising the reliability of the trained neural network. Motivated by this line of research, we present a contrastive methodology for assessing the reliability of representations produced by the proposed neural model. Denote the set of representations corresponding quantum states as $\{\mathbf{r}_{\rho_1}, \mathbf{r}_{\rho_2}, \dots, \mathbf{r}_{\rho_n}\}$. We leverage reachability distances, $\{d_{\rho_j}\}_{j=1}^n$, derived from the OPTICS (Ordering Points To Identify the Clustering Structure) clustering algorithm [51] to evaluate the reliability of representations, denoted as $\{rv_{\rho_j}\}_{j=1}^n$:

$$\{d_{\rho_j}\}_{j=1}^n = \text{OPTICS}(\{\phi(\mathbf{r}_{\rho_j})\}_{j=1}^n),$$

$$rv_{\rho_j} = \frac{\exp(-d_{\rho_k})}{\max_{k=1}^n \exp(-d_{\rho_k})},$$

where ϕ is a feature encoder. In the OPTICS clustering algorithm, a smaller reachability distance indicates that the associated point lies closer to the center of its corresponding cluster, thereby facilitating its clustering process. Intuitively, a higher density within a specific region of the representation space indicates that the trained neural model has had more opportunities to gather information from that area, thus enhancing its reliability. Our proposed method is supported by similar concepts introduced in [50]. More details are provided in Supplementary Note 3.

Prediction Network. For each type of property associated with the state, we employ a dedicated prediction network responsible for making predictions. Each prediction network is composed of three MLPs. The first MLP takes the state representation \mathbf{r}_ρ as input and transforms it into a feature vector \mathbf{h}^r while the second takes the query task index q as input and transforms it into a feature vector \mathbf{h}^q . The second MLP operates on the combined feature vectors $[\mathbf{h}^r, \mathbf{h}^q]$ to produce the prediction $f_q(\rho)$ for the property under consideration:

$$\begin{aligned} \mathbf{h}^r &= \text{MLP}_4(\mathbf{r}_\rho), \\ \mathbf{h}^q &= \text{MLP}_5(q), \\ f_q(\rho) &= \text{MLP}_6([\mathbf{h}^r, \mathbf{h}^q]). \end{aligned}$$

Network training. We employ the stochastic gradient descent [52] optimization algorithm and the Adam optimizer [53] to train our neural network. In our training procedure, for each state within the training dataset, we jointly train both the representation network and the prediction networks associated with one or two types of properties available for that specific state. This training is achieved by minimizing the difference between the predicted values generated by the network and the ground-truth values, thus refining the model's ability to capture and reproduce the desired property characteristics. The detailed pseudocode for the training process can be found in Supplementary Note 2.

Hardware. We employ the PyTorch framework [54] to construct the multi-task neural networks in all our experiments and train them with two NVIDIA GeForce GTX 1080 Ti GPUs.

Acknowledgements. We thank Ge Bai, Dong-Sheng Wang, Shuo Yang and Yuchen Guo for the helpful discussions on many-body quantum systems. This work was supported by funding from the Hong Kong Research Grant Council through grants no. 17300918 and no. 17307520, through the Senior Research Fellowship Scheme SRFS2021-7S02, and the John Templeton Foundation through grant 62312, The Quantum Information Structure of Spacetime (qiss.fr). YXW acknowledges funding from the National Natural Science Foundation of China through grants no. 61872318. Research at the Perimeter Institute is supported by the Government of Canada through the Department of Innovation, Science and Economic Development Canada and by the Province of Ontario through the Ministry of Research, Innovation and Science. The opinions expressed in this publication

are those of the authors and do not necessarily reflect the

views of the John Templeton Foundation.

-
- [1] Giacomo Torlai, Guglielmo Mazzola, Juan Carrasquilla, Matthias Troyer, Roger Melko, and Giuseppe Carleo, “Neural-network quantum state tomography,” *Nat. Phys.* **14**, 447–450 (2018).
 - [2] Juan Carrasquilla, Giacomo Torlai, Roger G Melko, and Leandro Aolita, “Reconstructing quantum states with generative models,” *Nat. Mach. Intell.* **1**, 155–161 (2019).
 - [3] Yan Zhu, Ya-Dong Wu, Ge Bai, Dong-Sheng Wang, Yuexuan Wang, and Giulio Chiribella, “Flexible learning of quantum states with generative query neural networks,” *Nat. Commun.* **13**, 6222 (2022).
 - [4] Tobias Schmale, Moritz Reh, and Martin Gärttner, “Efficient quantum state tomography with convolutional neural networks,” *NPJ Quantum Inf.* **8**, 115 (2022).
 - [5] Giuseppe Carleo and Matthias Troyer, “Solving the quantum many-body problem with artificial neural networks,” *Science* **355**, 602–606 (2017).
 - [6] Xiaoqian Zhang, Maolin Luo, Zhaodi Wen, Qin Feng, Shengshi Pang, Weiqi Luo, and Xiaoqi Zhou, “Direct fidelity estimation of quantum states using machine learning,” *Phys. Rev. Lett.* **127**, 130503 (2021).
 - [7] Tailong Xiao, Jingzheng Huang, Hongjing Li, Jianping Fan, and Guihua Zeng, “Intelligent certification for quantum simulators via machine learning,” *NPJ Quantum Inf.* **8**, 138 (2022).
 - [8] Yuxuan Du, Yiibo Yang, Tongliang Liu, Zhouchen Lin, Bernard Ghanem, and Dacheng Tao, “Shadownet for data-centric quantum system learning,” arXiv preprint arXiv:2308.11290 (2023).
 - [9] Ya-Dong Wu, Yan Zhu, Ge Bai, Yuexuan Wang, and Giulio Chiribella, “Quantum similarity testing with convolutional neural networks,” *Phys. Rev. Lett.* **130**, 210601 (2023).
 - [10] Yang Qian, Yuxuan Du, Zhenliang He, Min-hsiu Hsieh, and Dacheng Tao, “Multimodal deep representation learning for quantum cross-platform verification,” arXiv preprint arXiv:2311.03713 (2023).
 - [11] Jun Gao, Lu-Feng Qiao, Zhi-Qiang Jiao, Yue-Chi Ma, Cheng-Qiu Hu, Ruo-Jing Ren, Ai-Lin Yang, Hao Tang, Man-Hong Yung, and Xian-Min Jin, “Experimental machine learning of quantum states,” *Phys. Rev. Lett.* **120**, 240501 (2018).
 - [12] Johnnie Gray, Leonardo Banchi, Abolfazl Bayat, and Sougato Bose, “Machine-learning-assisted many-body entanglement measurement,” *Phys. Rev. Lett.* **121**, 150503 (2018).
 - [13] Dominik Koutný, Laia Ginés, Magdalena Moczala-Dusanowska, Sven Höfling, Christian Schneider, Ana Predojević, and Miroslav Ježek, “Deep learning of quantum entanglement from incomplete measurements,” *Sci. Adv.* **9**, eadd7131 (2023).
 - [14] Giacomo Torlai, Brian Timar, Evert P. L. van Nieuwenburg, Harry Levine, Ahmed Omran, Alexander Keesling, Hannes Bernien, Markus Greiner, Vladan Vuletić, Mikhail D. Lukin, Roger G. Melko, and Manuel Endres, “Integrating neural networks with a quantum simulator for state reconstruction,” *Phys. Rev. Lett.* **123**, 230504 (2019).
 - [15] Yulei Huang, Liangyu Che, Chao Wei, Feng Xu, Xinfang Nie, Jun Li, Dawei Lu, and Tao Xin, “Measuring quantum entanglement from local information by machine learning,” arXiv preprint arXiv:2209.08501 (2022).
 - [16] Murali K. Kurmapu, V.V. Tiunova, E.S. Tiunov, Martin Ringbauer, Christine Maier, Rainer Blatt, Thomas Monz, Aleksey K. Fedorov, and A.I. Lvovsky, “Reconstructing complex states of a 20-qubit quantum simulator,” *PRX Quantum* **4**, 040345 (2023).
 - [17] Alistair W. R. Smith, Johnnie Gray, and M. S. Kim, “Efficient quantum state sample tomography with basis-dependent neural networks,” *PRX Quantum* **2**, 020348 (2021).
 - [18] Juan Carrasquilla and Roger G Melko, “Machine learning phases of matter,” *Nat. Phys.* **13**, 431–434 (2017).
 - [19] Evert PL Van Nieuwenburg, Ye-Hua Liu, and Sebastian D Huber, “Learning phase transitions by confusion,” *Nat. Phys.* **13**, 435–439 (2017).
 - [20] Patrick Huembeli, Alexandre Dauphin, and Peter Wittek, “Identifying quantum phase transitions with adversarial neural networks,” *Phys. Rev. B* **97**, 134109 (2018).
 - [21] Benno S Rem, Niklas Käming, Matthias Tarnowski, Luca Asteria, Nick Fläschner, Christoph Becker, Klaus Sengstock, and Christof Weitenberg, “Identifying quantum phase transitions using artificial neural networks on experimental data,” *Nat. Phys.* **15**, 917–920 (2019).
 - [22] Korbinian Kottmann, Patrick Huembeli, Maciej Lewenstein, and Antonio Acín, “Unsupervised phase discovery with deep anomaly detection,” *Phys. Rev. Lett.* **125**, 170603 (2020).
 - [23] Frank Pollmann and Ari M. Turner, “Detection of symmetry-protected topological phases in one dimension,” *Phys. Rev. B* **86**, 125441 (2012).
 - [24] Hsin-Yuan Huang, Richard Kueng, and John Preskill, “Predicting many properties of a quantum system from very few measurements,” *Nat. Phys.* **16**, 1050–1057 (2020).
 - [25] Hsin-Yuan Huang, “Learning quantum states from their classical shadows,” *Nat. Rev. Phys.* **4**, 81–81 (2022).
 - [26] Andreas Elben, Steven T Flammia, Hsin-Yuan Huang, Richard Kueng, John Preskill, Benoît Vermersch, and Peter Zoller, “The randomized measurement toolbox,” *Nat. Rev. Phys.* **5**, 9–24 (2023).
 - [27] Haimeng Zhao, Laura Lewis, Ishaan Kannan, Yihui Quek, Hsin-Yuan Huang, and Matthias C Caro, “Learning quantum states and unitaries of bounded gate complexity,” arXiv preprint arXiv:2310.19882 (2023).
 - [28] Marcus Cramer, Martin B Plenio, Steven T Flammia, Rolando Somma, David Gross, Stephen D Bartlett, Olivier Landon-Cardinal, David Poulin, and Yi-Kai Liu, “Efficient quantum state tomography,” *Nat. Commun.* **1**, 149 (2010).
 - [29] Tillmann Baumgratz, Alexander Nüfeler, Marcus Cramer, and Martin B Plenio, “A scalable maximum likelihood method for quantum state tomography,” *New J. Phys.* **15**, 125004 (2013).
 - [30] BP Lanyon, C Maier, Milan Holzäpfel, Tillmann Baumgratz, C Hempel, P Jurcevic, Ish Dhand, AS Buyskikh,

- AJ Daley, Marcus Cramer, *et al.*, “Efficient tomography of a quantum many-body system,” *Nat. Phys.* **13**, 1158–1162 (2017).
- [31] Yuchen Guo and Shuo Yang, “Scalable quantum state tomography with locally purified density operators and local measurements,” arXiv:2307.16381 (2023).
- [32] Yu Zhang and Qiang Yang, “A survey on multi-task learning,” *IEEE Trans. Knowl. Data Eng.* **34**, 5586–5609 (2021).
- [33] Alexander A Klyachko, “Quantum marginal problem and n-representability,” in *Journal of Physics: Conference Series*, Vol. 36 (IOP Publishing, 2006) p. 72.
- [34] Matthias Christandl and Graeme Mitchison, “The spectra of quantum states and the kronecker coefficients of the symmetric group,” *Communications in Mathematical Physics* **261**, 789–797 (2006).
- [35] Christian Schilling, “The quantum marginal problem,” in *Mathematical Results in Quantum Mechanics: Proceedings of the QMath12 Conference* (World Scientific, 2015) pp. 165–176.
- [36] Pietro Smacchia, Luigi Amico, Paolo Facchi, Rosario Fazio, Giuseppe Florio, Saverio Pascazio, and Vlatko Vedral, “Statistical mechanics of the cluster ising model,” *Phys. Rev. A* **84**, 022304 (2011).
- [37] Iris Cong, Soonwon Choi, and Mikhail D Lukin, “Quantum convolutional neural networks,” *Nat. Phys.* **15**, 1273–1278 (2019).
- [38] Johannes Herrmann, Sergi Masot Lima, Ants Remm, Petr Zapletal, Nathan A McMahon, Colin Scarato, François Swiadek, Christian Kraglund Andersen, Christoph Hellings, Sebastian Krinner, *et al.*, “Realizing quantum convolutional neural networks on a superconducting quantum processor to recognize quantum phases,” *Nat. Commun.* **13**, 4144 (2022).
- [39] Paul R Cohen and Adele E Howe, “How evaluation guides ai research: The message still counts more than the medium,” *AI magazine* **9**, 35–35 (1988).
- [40] Hsin-Yuan Huang, Richard Kueng, Giacomo Torlai, Victor V Albert, and John Preskill, “Provably efficient machine learning for quantum many-body problems,” *Science* **377**, eabk3333 (2022).
- [41] Yu-Jie Liu, Adam Smith, Michael Knap, and Frank Pollmann, “Model-independent learning of quantum phases of matter with quantum convolutional neural networks,” *Phys. Rev. Lett.* **130**, 220603 (2023).
- [42] Andreas Elben, Jinlong Yu, Guanyu Zhu, Mohammad Hafezi, Frank Pollmann, Peter Zoller, and Benoît Vermersch, “Many-body topological invariants from randomized measurements in synthetic quantum matter,” *Sci. Adv.* **6**, eaaz3666 (2020).
- [43] Andreas Elben, Benoît Vermersch, Rick van Bijnen, Christian Kokail, Tiff Brydges, Christine Maier, Manoj K. Joshi, Rainer Blatt, Christian F. Roos, and Peter Zoller, “Cross-platform verification of intermediate scale quantum devices,” *Phys. Rev. Lett.* **124**, 010504 (2020).
- [44] Mark Fannes, Bruno Nachtergaele, and Reinhard F Werner, “Finitely correlated states on quantum spin chains,” *Commun. Math. Phys.* **144**, 443–490 (1992).
- [45] David Perez-García, Frank Verstraete, Michael M Wolf, and J Ignacio Cirac, “Matrix product state representations,” *Quantum Inf. Comput.* **7**, 401–430 (2007).
- [46] Ulrich Schollwöck, “The density-matrix renormalization group,” *Rev. Mod. Phys.* **77**, 259 (2005).
- [47] Matt W Gardner and SR Dorling, “Artificial neural networks (the multilayer perceptron)—a review of applications in the atmospheric sciences,” *Atmospheric environment* **32**, 2627–2636 (1998).
- [48] Junyoung Chung, Caglar Gulcehre, Kyunghyun Cho, and Yoshua Bengio, “Empirical evaluation of gated recurrent neural networks on sequence modeling,” in *NIPS 2014 Workshop on Deep Learning, December 2014* (2014).
- [49] Kimin Lee, Kibok Lee, Honglak Lee, and Jinwoo Shin, “A simple unified framework for detecting out-of-distribution samples and adversarial attacks,” *Advances in neural information processing systems* **31** (2018).
- [50] Yiyu Sun, Yifei Ming, Xiaojin Zhu, and Yixuan Li, “Out-of-distribution detection with deep nearest neighbors,” in *International Conference on Machine Learning* (PMLR, 2022) pp. 20827–20840.
- [51] Mihael Ankerst, Markus M Breunig, Hans-Peter Kriegel, and Jörg Sander, “Optics: Ordering points to identify the clustering structure,” *ACM Sigmod record* **28**, 49–60 (1999).
- [52] Léon Bottou, “Stochastic gradient descent tricks,” in *Neural Networks: Tricks of the Trade: Second Edition* (Springer, 2012) pp. 421–436.
- [53] Diederik P Kingma and Jimmy Ba, “Adam: A method for stochastic optimization,” arXiv preprint arXiv:1412.6980 (2014).
- [54] Adam Paszke, Sam Gross, Francisco Massa, Adam Lerer, James Bradbury, Gregory Chanan, Trevor Killeen, Zeming Lin, Natalia Gimelshein, Luca Antiga, *et al.*, “Pytorch: An imperative style, high-performance deep learning library,” *Advances in neural information processing systems* **32** (2019).